Sensorless Predictive Torque Control of PM-Assissted Synchronous Reluctance Machine Using Extended Kalman Filter and Adaptive Filter

Ali Sarajian[1], Davood Arab khaburi[2], Mohsen Siami[3], Alireza Abbaszadeh[4]
Department of Electrical Engineering, Iran University of Science & Technology, Tehran, Iran
Emali:asarajian@alumni.iust.ac.ir[1] khaburi@iust.ac.ir[2] siami@iust.ac.ir[3] a_abbaszadeh@iust.ac.ir[4]

Abstract: *The Permanent Magnet-Assisted Synchronous Reluctance Motor (PMA-SynRM) drive has become one of the most interesting replacements for the high efficiency variable speed drive. Herein, sensorless predictive torque control of a PMA-SynRM with non-sinusoidal back electromotive force (Back-EMF) is introduced. In order to control PMA-SynRM, finite control set-model predictive control (FCS-MPC) is implemented by means of a two-level inverter. Furthermore, an improved form of FCS-MPC, i.e., direct mean torque control (DMTC), is utilized as a second method to control PMA-SynRM. For improving the sensorless the combination of Extended Kalman Filter (EKF), Adaptive Filter (AF) and quadrature Phase-Locked Loop (PLL) are used for better estimation of the non-sinusoidal back EMF, elimination of the high order harmonics, and the accurate estimation of position and speed rotor, respectively. The simulations in nominal and low speed conditions result in effectively minimizing torque ripples compared to conventional FCS-MPC. The outcomes of the observer simulation are successfully guaranteed the accurate estimation of speed and rotor position.*

Key words: *Permanent Magnet Assissted Synchronous Reluctance Motor, Extended Kalman Filter, Adaptive Filter, Predictive Torque Control, Direct Mean Torque Control*

I. INTRODUCTION

Permanent-Magnet Assisted Synchronous Reluctance Machines (PMA-SynRMs) are known for application in high-efficiency adjustable speed drives (ASDs). These ASDs utilize electromagnetic torque consisting reluctance and the permanent magnet components to achieve this purpose. The amount of magnets and the magnet flux linkages are small in comparison with the conventional Interior Permanent-Magnet Motors (IPMs), and the reluctance torque has the most contribution in the produced torque. Compared with the conventional Synchronous reluctance machines (SynRMs), the PMA-SynRMs increase efficiency and power density. Altogether, the good characteristics of SynRMs and Permanent-Magnet motors are gathered in PMA-SynRMs [1]–[4].

Conventional direct torque control (DTC) is a modern control method that illustrates a good dynamic behavior. This method selects the active voltage vector (AVV) and the zero voltage vector (ZVV) by using a switching table [5]–[7]. However, this method has some disadvantages. The most important ones are switching frequency variation and considerable torque ripple. To tackle these problems, a direct mean torque control (DMTC) and then an improved algorithm of DMTC were proposed for SynRM [8]. Moreover, DTC by using space vector modulation [9], Band-constraining DTC [10], and predictive DTC [11] are proposed methods for reducing the torque ripple.

Finite control set predictive torque control (FCS-PTC) is an effective method. The FCS-PTC method calculates all possible voltage vectors within one sampling interval and selects the best one by using an optimization cost function [12]. The PTC method along with DMTC method have been used in

SynRM [13] and PMSM [14]. Furthermore, the combination of FCS-PTC and DMTC are implemented in induction machine (IM) [15]. To use predictive control, we need accurate model of machine. The PTC method unlike the DTC method is not inherently sensorless, consequently the state variables of machine should be estimated using observer [16].

The main source of torque pulsation in the machine is existence of the harmonic components of the air gap flux [17], [18]. Rotational motion of the magnet through the air gap results in nonsinusoidial flux density in the stator tooth and yoke. These harmonic components include the fifth and seventh harmonic [19]. In order to estimate the air gap flux, Luenberger observer [20], model reference adaptive system [21], sliding mode observer [22] and extended kalman filter [23] have been used for IMs. Inaccurate estimate of rotor position is due to the harmonics in the air gap flux. So, in order to eliminate the harmonic components, an adaptive filter should be used [24]. In recent years, the use of adaptive filters has shown a powerful technique to perform the extraction of the sinusoidal waveform while separating the harmonic components [25]–[27]. Adaptive filter detects the fifth and seventh harmonic components based on recursive least square (RLS) and least mean square (LMS) algorithm [28]. In addition, to reduce the influence of errors in estimating speed and position of the rotor, the phase lock loop (PLL) should be used rather than arc-tangent function. PLL can generate harmonics inphase with a reference wave in a manner that its stability is the same as the reference wave stability [29], [30].

Sensorless vector-control for PMA–SynRM using sliding mode observer has been presented in [31], [32]. Also, Sensorless direct torque and flux control with space vector modulation (DTFC–SVM) for PMA–SynRM has been successfully implemented in a sliding-mode approach [33]. This paper presents sensorless FCS-PTC method with improved DMTC for achieving low torque ripples of PMA-SynRM with nonsinusoidial back electromotive force based on extended kalman filter, adaptive filter and PLL. Simulation results using Matlab/Simulink show the validity of the proposed control method and observer scheme as well as the excellent dynamic response of the electromagnetic torque, low torque ripples and enhance the performance of the observers in wide speed rang.

II. MODEL PREDICTIVE TORQUE CONTROL OF PMA-SYNRM

A. PMA-SynRM model

The voltage equation of a PMA-SynRM in the synchronous reference frame can be expressed as follows:

$$\begin{aligned} u_{qs} &= R_s i_{qs} + \frac{d\psi_{qs}}{dt} + \omega_e \psi_{ds} \\ u_{ds} &= R_s i_{ds} + \frac{d\psi_{ds}}{dt} - \omega_e \psi_{qs} \end{aligned} \tag{1}$$

where, R_S is stator resistance and ω_e is electrical rotor angular speed, u_{ds} and u_{qs} are the d and q-axes voltages, and i_{ds} and i_{qs} are the d and q-axes currents. Ψ_{qs} and Ψ_{ds} are stator flux components in d and q-axes. Rotor nonsinusoidal flux distribution produces two new components: Ψ_{qm} and Ψ_{dm} that are the rotor flux linkages in d and q axes, respectively. Stator flux equations of the PMA-SynRM in the d-q reference frame are expressed as follows:

$$\begin{aligned} \psi_{qs} &= L_q i_{qs} - \psi_m - \psi_m \times \\ &\sum_{n=1}^{\infty} \left(K_{6n-1} + K_{6n+1}\right) \cos\left(6n\theta\right) = L_q i_{qs} - \psi_{qm} \end{aligned} \tag{2}$$

$$\begin{aligned} \psi_{ds} &= L_d i_{ds} - \psi_m \times \\ &\sum_{n=1}^{\infty} \left(K_{6n-1} + K_{6n+1}\right) \sin\left(6n\theta\right) = L_d i_{ds} - \psi_{dm} \end{aligned} \tag{3}$$

If the back EMF harmonics higher than sixth order are negligible, the back EMF equations i.e., e_{ds} and e_{qs} that are the d and q-axes back EMFs, are given as fallow:

$$e_{qs} = \omega_e \psi_{qm} = E_1 + E_6 \cos\left(6\theta\right) \tag{4}$$

$$e_{ds} = \omega_e \psi_{dm} = E_6 \sin(6\theta) \quad (5)$$

where, E_1 and E_6 are the amplitude of the fundamental component and sixth order harmonic of the back EMFs, in the synchronous reference frame due to the nonsinusoidal rotor flux, respectively. According to (2)-(5), (1) can be rearranged as

$$\begin{aligned} u_{qs} &= R_s i_{qs} + L_q \frac{di_{qs}}{dt} - \frac{d\psi_{qm}}{dt} + \omega_e L_d i_{ds} - e_{ds} \\ u_{ds} &= R_s i_{ds} + L_d \frac{di_{ds}}{dt} + \frac{d\psi_{dm}}{dt} - \omega_e L_q i_{qs} + e_{qs} \end{aligned} \quad (6)$$

where, L_d and L_q are d and q-axes inductances, respectively. Since the rotor flux can not vary sharply, the derivative of rotor flux components are zero $(d\psi_{qm}/dt = 0, d\psi_{dm}/dt = 0)$.

Now the electromagnetic torque can be defined as fallows:

$$\begin{aligned} T &= \frac{3}{2}\frac{p}{2}\left(\psi_{ds} i_{qs} - \psi_{qs} i_{ds}\right) \\ &= \frac{3}{2}\frac{p}{2}\left(\left(L_d i_{ds} - e_{ds}/\omega_e\right) i_{qs} \right. \\ &\qquad \left. - \left(L_q i_{qs} - e_{qs}/\omega_e\right) i_{ds}\right) \\ &= \frac{3}{2}\frac{p}{2}\left(\psi_{qm} i_{ds} - \psi_{dm} i_{qs} + \left(L_d - L_q\right) i_{ds} i_{qs}\right) \end{aligned} \quad (7)$$

B. Improved DMTC

Direct mean torque control (DMTC) was introduced to control the mean value of the torque at reference value [14]. Fig. 1 shows a typical cycle of operation of the improved DMTC. In this method, the interval switching time are divided into two segments including AVV and ZVV. Formerly, when AVV applies the torque increment occurs at the beginning cycle. Following, the reaching to virtual hysteresis width ΔT, ZVV applies and the torque decreases. In the steady state, the value of T_n at the beginning of a cycle should be equal to its value T_{n+1} at the end. The hatch area in Fig. 1, shows the torque response during the cycle of *n*. The value of the torque at the end of the cycle T_{n+1} can be described directly by the following formula:

$$\begin{aligned} T_{n+1} &= T_n + \frac{dT_{AVV}}{dt} t_{AVV} + \frac{dT_{ZVV}}{dt}\left(T_s - t_{AVV}\right) \\ &= T^* - \frac{1}{2}\Delta T \end{aligned} \quad (8)$$

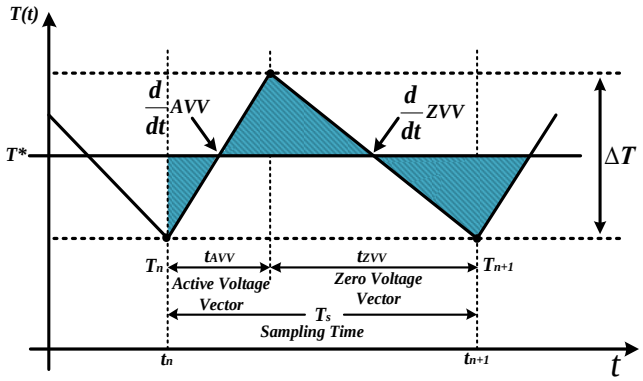

Fig. 1. Typical operation cycle of DMTC in steady state.

The virtual hysteresis width ΔT can be expressed:

$$\Delta T = \frac{dT_{AVV}}{dt} t_{AVV} = -\frac{dT_{ZVV}}{dt}\left(T_s - t_{AVV}\right) \quad (9)$$

By eliminating t_{AVV} in (9), virtual hysteresis width (ΔT) can be calculated from (10), as follows:

$$\Delta T = -\frac{\frac{dT_{AVV}}{dt}\frac{dT_{ZVV}}{dt}}{\frac{dT_{AVV}}{dt} - \frac{dT_{ZVV}}{dt}} T_s \quad (10)$$

(11) can be derived from inserting (10) to (8); thus:

$$\begin{aligned} t_{AVV} &= \frac{T^* - T - \frac{1}{2}\Delta T - \frac{dT_{ZVV}}{dt} T_s}{\frac{dT_{AVV}}{dt} - \frac{dT_{ZVV}}{dt}} \\ t_{ZVV} &= T_s - t_{AVV} \end{aligned} \quad (11)$$

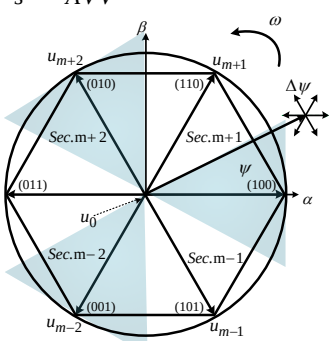

Fig. 2. Voltage space vectors, sectors and stator flux variation.

As can be seen in Fig. 2, in two-level inverter, the six possible AVVs have different effects on the flux as well as on the torque. With respect to improved DMTC, it is assumed that the stator flux vector (Ψ) is situated in the *m*th sector (m =1,...,6) of the α−β plane (Fig. 2) for positive rotation (ω >0). The two most favorable voltage vectors are preselected, and thus calculating t_{AVV} for both of them. For increasing the value of ψ, the AVVs u_{m+1} can be selected, while selecting u_{m+2} results in decreasing its magnitude. It should be noted that the value of T increases irrelevant from the number of sectors.

C. Calculation of the Torque Slopes

DT/dt can be determined by differentiating (7), as shown in (12):

$$\frac{dT}{dt}=\frac{3}{2}\frac{P}{2}\left(\psi_{qm}\frac{di_{ds}}{dt}-\psi_{dm}\frac{di_{qs}}{dt}+\left(L_{ds}-L_{qs}\right)\left(i_{ds}\frac{di_{qs}}{dt}+i_{q}\frac{di_{ds}}{dt}\right)\right) \tag{12}$$

From (12) and (6) and by supposing that a ZVV is exerted to the motor, the torque decreases, and its time derivative is obtained as follows:

$$\begin{aligned}\frac{dT_{ZVV}}{dt}=&\frac{3}{2}\frac{P}{2}\left[\psi_{qm}\left(\frac{-R_s i_{ds}+\omega_e L_q i_{qe}-\omega_e\psi_{qm}}{L_d}\right)\right.\\&-\psi_{dm}\left(\frac{-R_s i_{qs}-\omega_e L_d i_{ds}-\omega_e\psi_{dm}}{L_q}\right)\\&+\left(L_d-L_q\right)\times\left(i_{ds}\frac{-R_s i_{qs}-\omega_e L_d i_{ds}-\omega_e\psi_{dm}}{L_q}\right.\\&\left.\left.+i_{qs}\frac{-R_s i_{ds}+\omega_e L_q i_{qs}-\omega_e\psi_{qm}}{L_d}\right)\right]\end{aligned} \tag{13}$$

Besides, for an AVV, the torque derivative is obtained as fallows:

$$\frac{dT_{AVV}}{dt}=\frac{3}{2}\frac{P}{2}\left[\psi_{qm}\left(\frac{u_{ds}}{L_d}\right)-\psi_{dm}\left(\frac{u_{qs}}{L_q}\right)+\left(L_d-L_q\right)\left(i_{ds}\frac{u_{qs}}{L_q}+i_{qs}\frac{u_{ds}}{L_d}\right)\right]+\frac{dT_{ZVV}}{dt} \tag{14}$$

Another criterion is required to determine which voltage vector should be exerted to the motor. This criterion is based on the predictive control which is addressing the minimizing the torque ripple as well as the flux ripple.

D. Torque and flux prediction

Fig. 3 is the block diagram of the proposed control structure. In order to decide the best voltage vector, the FCS-PTC approach can be applied. In this approach a cost function that is the evaluation criterion to decide which AVV is the best to be applied. Because the torque and flux are the control variables in DMTC method, the cost function is defined as fallows:

$$J_m=\frac{1}{2}\left(\left|T_{k+1}-T^*\right|^2+K_\psi\left|\left|\psi_{s,k+1}\right|^2-\psi_s^{*2}\right|^2\right) \tag{15}$$

where, T_{k+1} and $\psi_{s,k+1}$ are the predicted values of torque and stator flux, respectively, and T^* and ψ^* are the reference values of torque and stator flux, respectively. K_ψ is a weighting factor that handles the relative importance between torque and stator flux control.

For small values of a control sampling time T_s, the d−q components of the stator current vector and stator flux vector can be predicted at the end of the switching interval By Euler's approximation of (1) and (6):

$$\begin{aligned}i_{ds,n+t_{AVV}}&=i_{ds,n}+t_{AVV}/L_d\left(u_d-R_s i_{ds}+\omega_e L_q i_{qs}-e_{qs}\right)\\i_{qs,n+t_{AVV}}&=i_{qs,n}+t_{AVV}/L_q\left(u_q-R_s i_{qs}-\omega_e L_d i_{ds}+e_{ds}\right)\end{aligned} \tag{16}$$

$$\begin{aligned}\psi_{ds,n+t_{AVV}}&=\psi_{ds,n}+t_{AVV}\left(u_d-R_s i_{ds}+\omega_e\psi_{qs}\right)\\\psi_{qs,n+t_{AVV}}&=\psi_{qs,n}+t_{AVV}\left(u_q-R_s i_{qs}-\omega_e\psi_{ds}\right)\end{aligned} \tag{17}$$

The torque prediction at the end of the same interval can be obtained by

$$T_{n+t_{AVV}} = \frac{3}{2}\frac{p}{2}\Big[\psi_{qm} i_{ds,n+t_{AVV}} - \psi_{dm} i_{qs,n+t_{AVV}} + \left(L_d - L_q\right) i_{ds,n+t_{AVV}}\, i_{qs,n+t_{AVV}}\Big] \quad (18)$$

With respect to the prediction of the torque and stator flux for every AVV and following by substituting them into the cost function, the AVV that minimizes the cost function is selected as the best voltage vector.

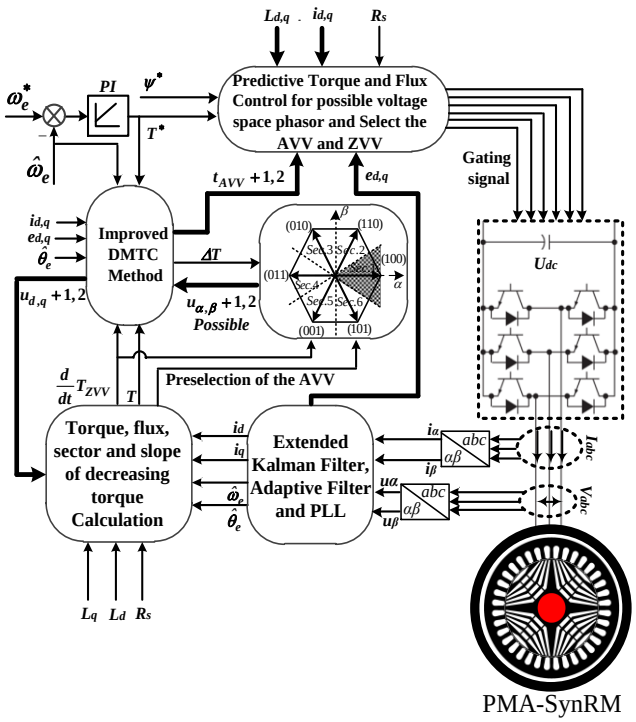

Fig. 3. Block diagram of the proposed FCS-PTC with improved DMTC for the PMA-SynRM.

E. Modeling of EKF estimator for back EMF estimation

Fig. 4 is the block diagram of the proposed observer structure. As considered before, the FCS-PTC method is dependent on speed and position of the rotor. Therefore, an observer is required to estimate the speed and position of the rotor. For estimation of the position, the air gap flux estimation is needed that is obtained by the Kalman Filter. This filter is an optimal stochastic method for state estimating and filtering in linear systems. For nonlinear systems, the Extended Kalman Filter should be considered [34], [35]. The state space equation can be described as follows:

$$\dot{x}(t) = f\left(x(t)\right) + Bu(t) + \sigma(t)$$
$$y(t) = Hx(t) + \mu(t) \quad (19)$$

where *x(t)*, *u(t)*, and *y(t)* are the states, inputs, and outputs of the system, respectively. The system noise $\sigma(t)$ and measurement noise $\mu(t)$ are supposed to be zero mean and white with Gaussian distributions of covariances *Q(t)* and *R(t)*, respectively. Once a nominal solution to the nonlinear (19) has been obtained, the linearized perturbation equations of the system are as follows:

$$\delta\dot{x}(t) = F\left(x(t)\right)\delta x(t) + B\,\delta u(t) + \sigma(t) \quad (20)$$

$$\delta y(t) = H\,\delta x(t) + \mu(t) \quad (21)$$

where, the Jacobian matrix (*F*) and output matrix (*H*) are determined in the following form:

$$F\left(x(t)\right) = \left.\frac{\partial f}{\partial x}\right|_{x=x(t)} \quad (22)$$

$$H\left(x(t)\right) = \left.\frac{\partial h}{\partial x}\right|_{x=x(t)} \quad (23)$$

The optimum state estimated sequence $\hat{x}_n$ is a minimum variance estimation of the *x(t)* that is obtained by the filter. Both the optimum state and its covariance P_n produced by the filter are put in a two-step loop. The EKF procedure can be defined by a two-step recursive algorithm.

The predicted estimation is attained from (20) and through a simple rectangular integration as [38]:

$$\hat{x}_{n|n-1} = \hat{x}_{n-1} + \left(F\left(\hat{x}_{n-1}\right) + Bu_{n-1}\right)T_s = \left(I + FT_s\right)\hat{x}_{n-1} + BT_s u_{n-1} \quad (24)$$

The estimation covariance can be predicted by

$$P_{n|n-1} = \phi_{n-1} P_{n-1} \phi_{n-1}^{'} + Q_d \quad (25)$$

According to (23) and by use of a rectangular integration, a new estimation and, consequently, its covariance are attained as:

$$\hat{x}_n = \hat{x}_{n|n-1} + K_n\left[y_n - H\hat{x}_{n|n-1}\right] \quad (26)$$

$$P_n = P_{n|n-1} - K_n H P_{n|n-1} \tag{27}$$

where, K and H that are respectively, the filter gain matrix and the transformation matrix are described by

$$\begin{aligned} K_n &= P_{n|n-1} H^{'} \left(H P_{n|n-1} H^{'} + R_d \right)^{-1} \\ H\left(x\left(t\right)\right) &= {\partial h\left(x\right)} \Big/ {\partial x} \Big| x = x_{n|n-1} \end{aligned} \tag{28}$$

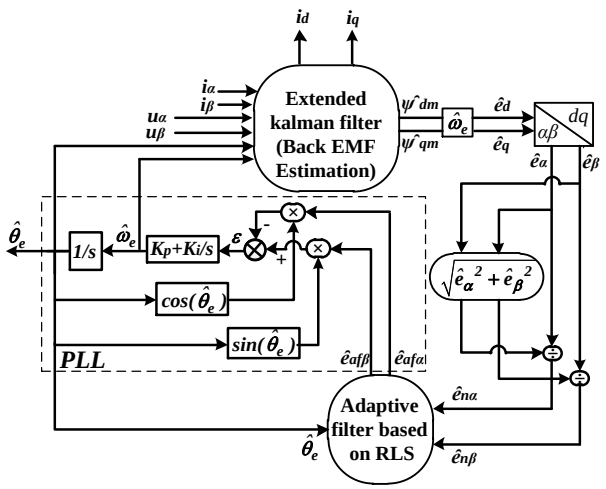

Fig. 4. EKF and AF with the quadrature PLL.

From (6), the PMA-SynRM voltage and the flux linkage can be defined in the rotor reference frames as fallows:

$$\begin{cases} \dfrac{di_d}{dt} = \dfrac{u_d}{L_d} - \dfrac{R_s}{L_d} i_d + \dfrac{L_q}{L_d} \omega_e i_q - \dfrac{\omega_e}{L_d} \psi_{qm} \\ \dfrac{di_q}{dt} = \dfrac{u_q}{L_q} - \dfrac{R_s}{L_q} i_q - \dfrac{L_d}{L_q} \omega_e i_d - \dfrac{\omega_e}{L_q} \psi_{dm} \\ \dfrac{d\psi_{dm}}{dt} = 0 \\ \dfrac{d\psi_{qm}}{dt} = 0 \end{cases} \tag{29}$$

F. Adaptive filter with PLL for compensation of position harmonic error

Following the estimation of the back EMF, speed and position of the rotor based on the arc tangent function is calculated from the below equations [36]–[39]:

$$\theta_e\left(n\right) = -\tan^{-1}\left(\hat{e}_\beta\left(n\right) / \hat{e}_\alpha\left(n\right)\right) \tag{30}$$

$$\begin{aligned} \omega_e\left(n\right) &= -\frac{d}{dt}\tan^{-1}\left(e_\beta\left(n\right) \Big/ e_\alpha\left(n\right) \right) \\ &= \frac{e_\beta\left(n\right)\frac{d}{dt}\left(e_\alpha\left(n\right)\right) - e_\alpha\left(n\right)\frac{d}{dt}\left(e_\beta\left(n\right)\right)}{e_\alpha^2\left(n\right) + e_\beta^2\left(n\right)} \end{aligned} \tag{31}$$

where, $\hat{e}_\alpha$ and $\hat{e}_\beta$ are the estimation back EMF in α and β-axes, respectively. It should be noted (30) and (31) suffer from the lack of the accuracy due to appearance of harmonic in air gap flux. In order to reduce the effect of estimation error, PLL was used as a replacement of arc tangent function. Because the back EMF changes in different speeds, the input estimation back EMF for the PLL is normalized [29]. The normalized error position of signal is calculated from the below equation as follows:

$$\varepsilon = \frac{1}{\sqrt{\hat{e}_\alpha^2 + \hat{e}_\beta^2}} \left[\hat{e}_\alpha \cos\left(\hat{\theta}_e\right) - \hat{e}_\beta \sin\left(\hat{\theta}_e\right) \right] \tag{32}$$

Therefore, the estimation of rotor position acquired from the PLL can be achieved as follows:

$$\hat{\theta}_e = \left(\frac{1}{s}\right)\left(\frac{k_i}{s} + k_p\right)\varepsilon \tag{33}$$

Considering the dominant fifth and seventh harmonic components of back EMF generated by air gap flux harmonics, the phase difference between actual rotor position and estimated rotor position of the PMA-SynRM can be expressed as [36]:

$$\varepsilon \approx \theta_e - \hat{\theta}_e + e_6 \sin\left(6\omega_e t + \theta_{e6}\right) \tag{34}$$

where, e_6 is the amplitude of the equivalent sixth back EMF harmonic and θ_{e6} is the initial phase. It is noticeable that there is an additive error in the phase difference due to the sixth back EMF harmonic. However, due to the widely bandwidth of the PLL, utilizing the type-II system will partially eliminate the sixth harmonic. In addition, the difficulty of design of the type-II system parameters to eliminate the sixth harmonic without influencing on the fundamental components is due to variation of the speed. Therefore, an adaptive filter (AF) with PLL is used for the effectiveness compensation of harmonics in back EMF [30].

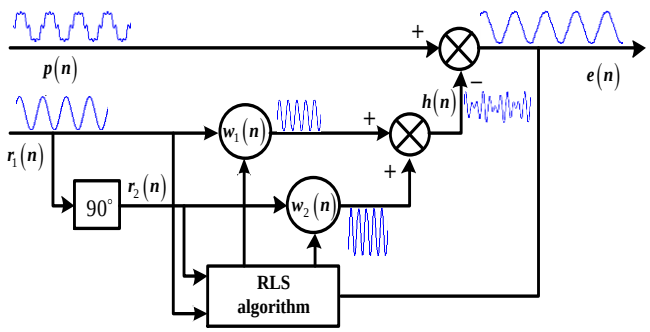

Fig. 5. Harmonic detection based on the adaptive filter

Wiener theory as a widely used kind of adaptive noise-cancelling method is an efficient method to eliminate the fifth and seventh harmonics of the back EMF estimations. This technique eliminates the given harmonic by self-tuning the filter coefficients with the adaptive method.

Fig. 5 depicts the theory of the harmonic eliminating on the base of the adaptive noise-cancelling technique with two orthogonal references for the position estimator. *p(n)* denotes the primary input which is comprised of a given signal and an additional harmonic signal. The two orthogonal signals, i.e., the first row and the second row of matrix *r(n)*, denote the harmonic references that the high-order harmonic components are converged to them. $w_1(n)$ and $w_2(n)$ are the adjustable filter coefficients corresponding to the harmonic references. The sum of these two weighted references form the output of filter *h(n)* that indicates the harmonic estimation. The fundamental component of desired signal is acquired from the error signal *e(n)* resulted from deducting *h(n)* from *p(n)*. Correspondingly, making the filter output *h(n)* to converge to the real high-order harmonic components is the objective of adaptive filter. Adjusting the filter coefficients is done by the RLS algorithm because of its fast convergence speed, [28].

The normalized estimations of back EMF, i.e., $\hat{e}_{n\alpha}$ and $\hat{e}_{n\beta}$, that are comprised of the fifth and seventh harmonic components, are multiplied by $\sin(5\hat{\theta}_e)$, $\cos(5\hat{\theta}_e)$ and $\sin(7\hat{\theta}_e)$, $\cos(7\hat{\theta}_e)$, respectively ($\hat{\theta}_e$ is the estimation of rotor position from the PLL output) are used for producing the AF harmonic references. $w_{ji}(n)$ and $k_{ji}(n)$ are coefficients and gains of the filter. The coefficients of filter can be adjusted by the RLS algorithm in a way that the fifth and seventh harmonic estimations converge to their actual values. The desirable fundamental components of the normalized back EMF is obtained as fallow:

$$\hat{e}_{af\,\alpha}(n)=\hat{e}_{n\alpha}-\sum_{i=1}^{2}\sum_{j=1}^{2}w_{ji}(n)r_{ji}(n) \tag{35}$$

$$\hat{e}_{af\,\beta}(n)=\hat{e}_{n\beta}-\sum_{i=3}^{4}\sum_{j=1}^{2}w_{ji}(n)r_{ji}(n) \tag{36}$$

where, $r_{ji}(n)$ imposes the harmonic reference signals and is given by the below matrix:

$$r(n)=\begin{bmatrix}\sin(5\hat{\theta}_e) & \sin(7\hat{\theta}_e) & \sin(5\hat{\theta}_e) & \sin(7\hat{\theta}_e)\\ \cos(5\hat{\theta}_e) & \cos(7\hat{\theta}_e) & \cos(5\hat{\theta}_e) & \cos(7\hat{\theta}_e)\end{bmatrix} \tag{37}$$

The meanings of $w_{ji}(n)$ is the estimation of the corresponding harmonic component magnitude, and it can be adjusted online according to the specification of the harmonic reference by the equations as follows:

$$w_{ji}(n)=w_{ji}(n-1)+k_{ji}(n)\hat{e}_{af\,\alpha}(n) \qquad j\ \&\ i=1,2 \tag{38}$$

$$w_{ji}(n)=w_{ji}(n-1)+k_{ji}(n)\hat{e}_{af\,\beta}(n) \qquad j=1,2\ \&\ i=3,4 \tag{39}$$

The gain vector $k_{ji}(n)$ can be calculated as follows:

$$k_{ji}(n)=\frac{\phi_{ji}(n)}{\lambda+r_{ji}(n)\phi_{ji}(n)} \qquad j=1,2\ \&\ i=1,2,3,4 \tag{40}$$

where, $\lambda\in(0,1)$ is the forgetting factor. With $\lambda = 1$, the conventional method of least squares can be achieved. The presence of λ is to guarantee that the data in the far apart past have less effect on the convergence. $\Phi_{ji}(n)$ is the intermediate variables that is obtained as follows:

$$\phi_{ji}(n)=P_{ji}(n-1)r_{ji}(n) \qquad j=1,2\ \&\ i=1,2,3,4 \tag{41}$$

The inverse of the autocorrelation matrix $P_{ji}(n)$ can be achieved as:

$$P_{ji}(n)=\lambda^{-1}\left(P_{ji}(n-1)-k_{ji}(n)\phi_{ji}(n)\right) \quad (42)$$
$$j=1,2\ \&\ i=1,2,3,4$$

The initial values of $w_{ji}(n)$ and $P_{ji}(n)$ are selected as:

$$P_{ji}(0)=\sigma, w_{ji}(0)=0 \quad j=1,2\ \&\ i=1,2,3,4 \quad (43)$$

It should be noticed that a smaller value of λ improves the tracking capability, but the stability of the RLS algorithm can be influenced. In this application, λ is set at 0.99995 and σ is chosen 0.001.

3. Simulation Results

In order to validate the proposed method to control of PMA-SynRM based EKF and AF, some simulations are done using Matlab¥Simulink software. Fig. 3 shows the predictive torque control scheme of the sensorless PMA-SynRM drive based on an EKF and AF with PLL. The parameters of the PMA-SynRM used in this paper are shown in TABLE 1. The sampling time of simulation is 50 μs.

TABLE I: Motor Parameters

Parameter	Value
P	4
R_S	1.25[Ω]
L_d	49.801[mH]
L_q	17.901[mH]
ψ_r	0.48[wb]
J_m	0.0012[kg.m^2]
B	0.0006[N.m.s]
ω_n	6000[rpm]
T_n	3.7[N.m]

Fig. 6 shows the actual and estimated d-axes and q-axes air gap flux linkage rotor. The motor rotates at 6000 rpm with rated load. The dotted lines shown in all Figurers express estimated results. At steady state, the mean value of the flux linkage estimation error at the d-axes and q-axes are 0.0308% and 0.0463%, respectively. From the presented result of EKF can be seen that the EKF showed the reliable and accurate performance.

Fig. 7 and 8 show the performance of AF in the α-axes and β-axes back EMF estimation with AF based on RLS at 6000 rpm with rated load. As can be seen in Fig. 5, back EMF estimates $\hat{e}_{n\alpha}$ directly obtained from the EKF. AF detected the fifth and seventh following by compensation of harmonic $\hat{e}_{5\alpha}$, $\hat{e}_{7\alpha}$ and leaded to estimate $\hat{e}_{af\alpha}$. The same situation is true for the β-axes (Fig.8).

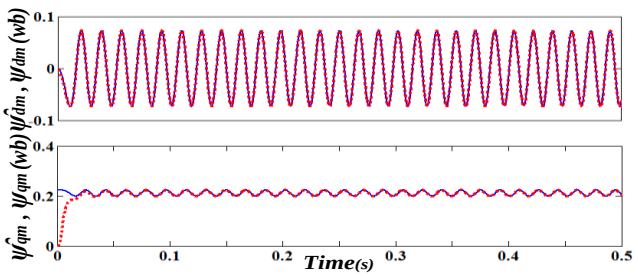

Fig. 6. Actual and estimated d-axes and q-axes flux linkage rotor.

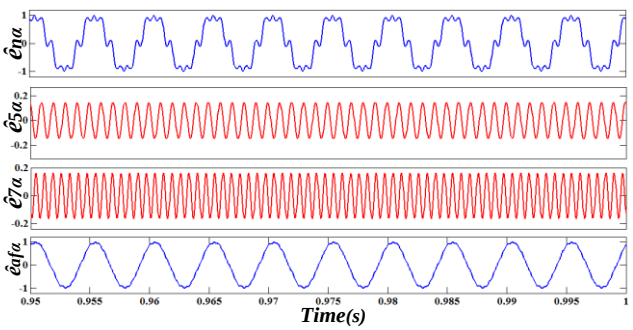

Fig. 7. The α-axes detection and compensation of normalized back EMF estimation.

The results of back EMF estimation become more sinusoidal with the proposed AF using the RLS algorithm, and the fifth and seventh harmonic distortions are effectively eliminated.

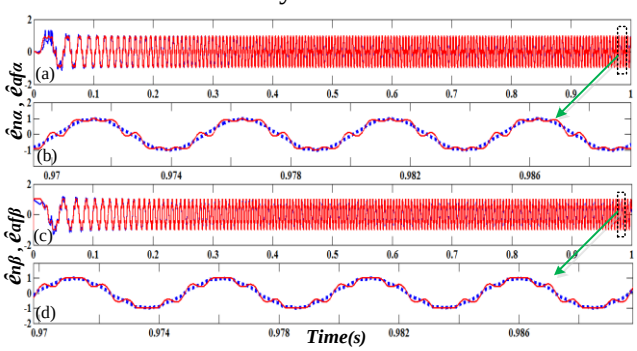

Fig. 8. The α-axes normalized back EMF estimation a) without AF and with AF. The β-axes normalized back EMF estimation c) without AF and with AF. b) and d) zoom of (a) and (c) respectively.

Fig. 9 shows the comparison of the estimated rotor position with arc tangent function and with the AF at 6000 rpm with rated load. It can be seen from Fig. 9(a), the estimated rotor position includes the sixth harmonic component, obviously. Notably in Fig. 9 (b), by utilizing the combination AF and PLL, the sixth harmonic component gets completely smooth and eliminated. Besides, the rotor position is accurately estimated and subsequently the mean value of the position estimation error is less than 1%, at the steady state.

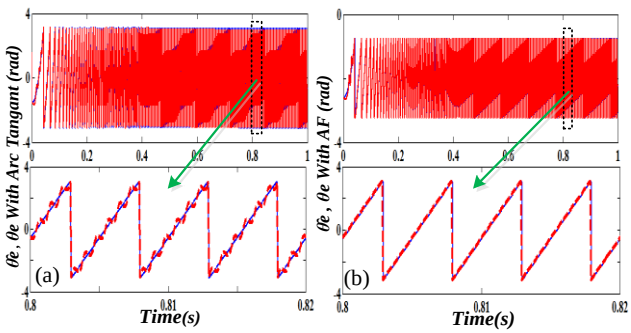

Fig. 9. Comparison of the actual and estimated position at 6000 rpm. a) with arc tangent function. b) with the AF.

Fig. 10 shows the actual and estimated speed of rotor using AF with PLL. The mean value of the speed estimation error is less than 0.51%, at the steady state.

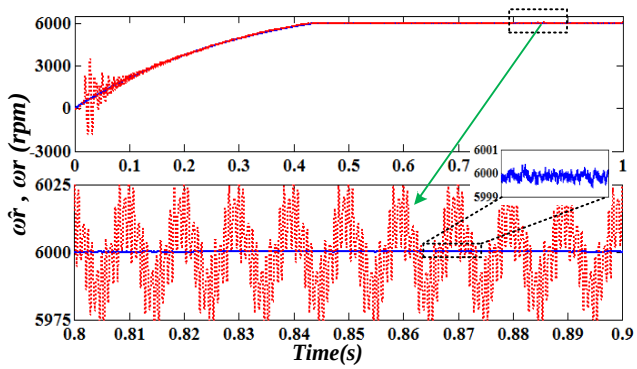

Fig. 10. Actual and estimated speed at 6000 rpm with rated load.

Fig. 11 and 12 demonstrate stator current and torque responses of the proposed conventional FCS-PTC and FCS-PTC method with improved DMTC, respectively. The conventional FCS-PTC method is modified by the proposed method in the view of torque ripple and total harmonic distortion (THD), for steady state.

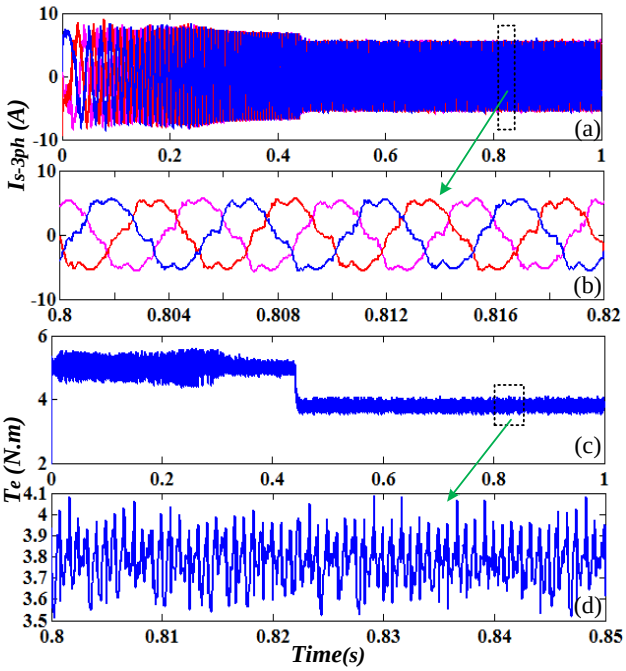

Fig. 11. Nominal torque step response of conventional FCS-PTC simulation result at 6000 rpm.

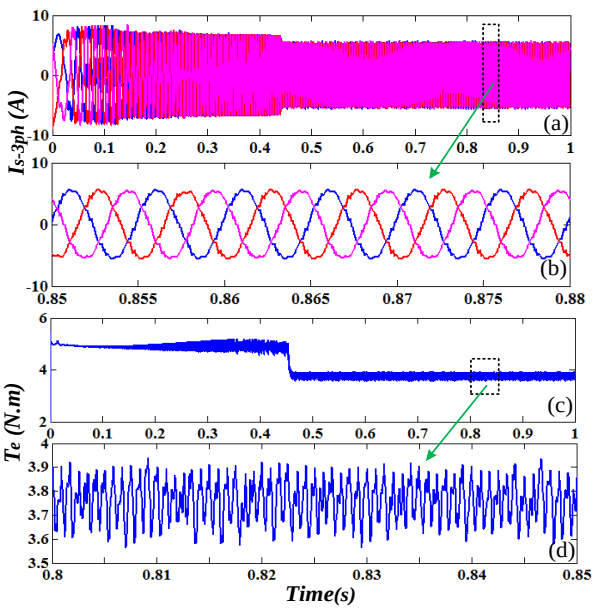

Fig. 12. Nominal torque step response of the conventional FCS-PTC with improved DMTC simulation result at 6000 rpm.

The torque ripple of conventional FCS-PTC and the THD of the stator current are 15.91 and 12.84%,

respectively, in switching frequency 4.804 KHZ. With regard to the proposed method the torque ripple and the THD of the stator current are 8.2 and 4.3%, respectively, in switching frequency 8.420 KHZ. As expected, torque ripple and the THD of the stator current will be reduced predominantly if the proposed method is utilized. It is should be mentioned that the speed of rotor is tracking the reference speed.

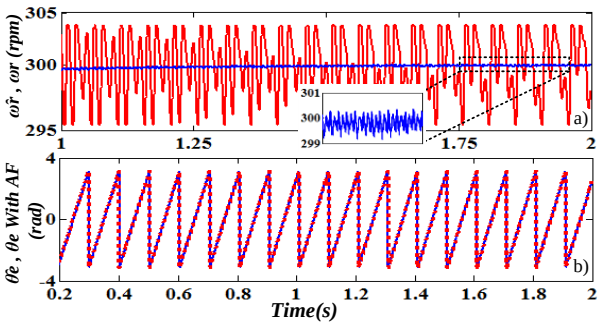

Fig. 13. A) actual and estimated speed, and b) actual and estimated position of the rotor at 300 rpm.

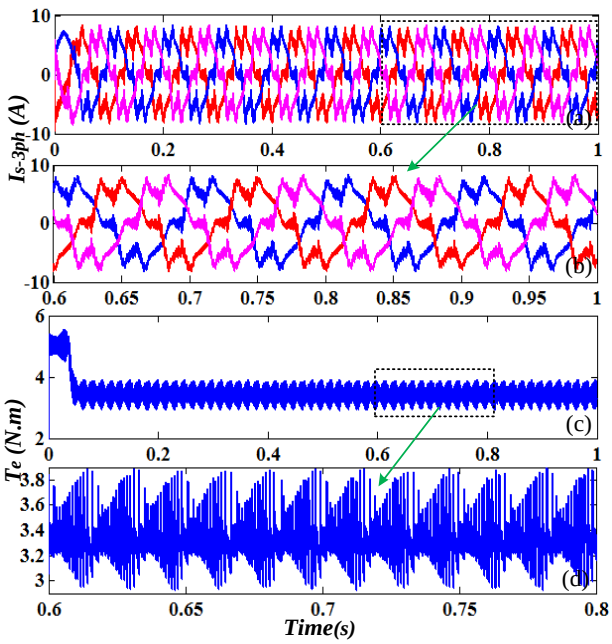

Fig. 14. Nominal torque step response of conventional FCS-PTC simulation result at 300 rpm.

Fig. 13(a) and (b) display actual and estimated speed and position of the rotor, respectively, at 300 rpm. As can be seen, the estimated rotor position is accurate and subsequently the mean value of the position estimation error is 0.91%, at the steady state. The mean value of the speed estimation error is 1.32%, at the steady state.

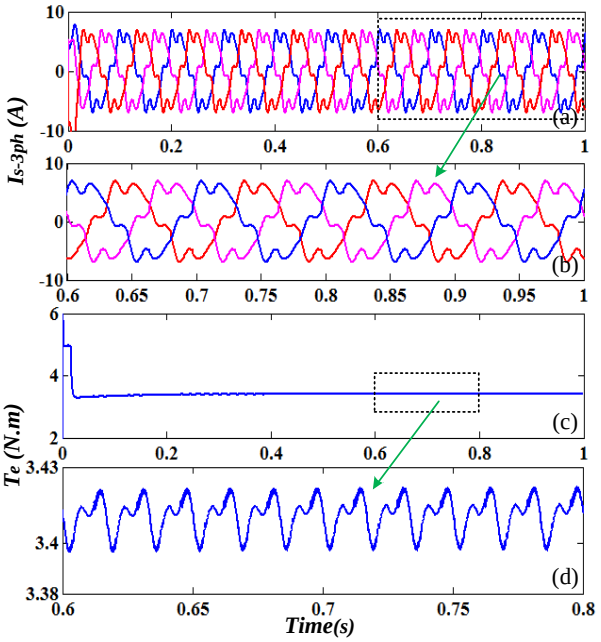

Fig. 15. Nominal torque step response of the conventional FCS-PTC with improved DMTC simulation result at 300 rpm.

Fig. 14 and 15 reveal stator current and torque responses of the proposed conventional FCS-PTC and FCS-PTC method with improved DMTC, respectively with rated load at 300 rpm. The torque ripple of conventional FCS-PTC and the THD of the stator current are 29.1 and 25.27%, respectively. With regard to the proposed method the torque ripple and the THD of the stator current are 2.31 and 20.17%, respectively. As expected, it is worth of mentioning that in this situation again the torque ripple and the THD of the stator current will be decreased effectively if the proposed method is used.

G. CONCLUSIONS

The presence of the harmonic components in air gap flux is the main source of the existence of torque ripple. The accurate performance of the machine is dependent on the variable parameters of the machine. Due to introducing the sensorlees control, the demand

of using observer is essential. Herein, a sensorless predictive torque control of PMA-SynRM with non-sinusoidal back EMF based on EKF and the combination of AF and PLL have been proposed.

The effectiveness of the proposed method has been verified accurately at a 2.3 kW PMA-SynRM sensorless drive. The simulation results demonstrate that the observer scheme including EKF, AF and PLL make an effective estimation of back EMF, the speed and position of the rotor. In both of nominal and low speed, the proposed method proved the promising results in the point of view of precise torque and speed control as well as the excellent dynamic response of the electromagnetic torque.

REFERENCES

[1] P. Niazi, H. a. Toliyat, D. H. Cheong, and J. C. Kim, "A low-cost and efficient permanent-magnet-assisted synchronous reluctance motor drive," IEEE Trans. Ind. Appl., vol. 43, no. 2, pp. 542–550, 2007.

[2] P. Niazi and H. a. Toliyat, "Online Parameter Estimation of Permanent-Magnet Assisted Synchronous Reluctance Motor," IEEE Trans. Ind. Appl., vol. 43, no. 2, pp. 609–615, 2007.

[3] W. H. Kim, K. S. Kim, S. J. Kim, D. W. Kang, S. C. Go, Y. Do Chun, and J. Lee, "Optimal PM design of PMA-SynRM for wide constant-power operation and torque ripple reduction," IEEE Trans. Magn., vol. 45, no. 10, pp. 4660–4663, 2009.

[4] S. Morimoto, M. Sanada, and Y. Takeda, "Performance of PM-assisted synchronous reluctance motor for high-efficiency and wide constant-power operation," IEEE Trans. Ind. Appl., vol. 37, no. 5, pp. 1234–1240, 2001.

[5] S. B. Ozturk, W. C. Alexander, and H. a. Toliyat, "Direct torque control of four-switch brushless dc motor with non-sinusoidal back emf," IEEE Trans. Power Electron., vol. 25, no. 2, pp. 263–271, 2010.

[6] F. Wang, Z. Zhang, S. Davari, R. Fotouhi, D. Arab Khaburi, J. Rodriguez, and R. Kennel, "An Encoderless Predictive Torque Control for an Induction Machine with a Revised Prediction Model and EFOSMO," IEEE Trans. Ind. Electron., vol. Early Acce, no. 12, pp. 6635–6644, 2014.

[7] T. Glasberger and V. Mužíková, "Sensorless Direct Torque Control of PMSM with Reduced Model Extended Kalman Filter," pp. 8239–8244.

[8] E. Flach, "Improved algorithm for direct mean torque control of an induction motor," in Proc. PCIM, Nuremberg, Germany, 1998, pp. 261–267.

[9] T. G. Habetler, F. Profumo, M. Pastorelli, and L. M. Tolbert, "Direct torque control of induction machines using space vector modulation," Industry Applications, IEEE Transactions on, vol. 28, no. 5. pp. 1045–1053, 1992.

[10] V. Ambrozic, G. S. Buja, and R. Menis, "Band-constrained technique for direct torque control of induction motor," Industrial Electronics, IEEE Transactions on, vol. 51, no. 4. pp. 776–784, 2004.

[11] J. Beerten, J. Verveckken, and J. Driesen, "Predictive Direct Torque Control for Flux and Torque Ripple Reduction," Industrial Electronics, IEEE Transactions on, vol. 57, no. 1. pp. 404–412, 2010.

[12] R. Vargas, J. Rodriguez, U. Ammann, and P. W. Wheeler, "Predictive Current Control of an Induction Machine Fed by a Matrix Converter With Reactive Power Control," IEEE Trans. Ind. Electron., vol. 55, no. 12, pp. 4362–4371, 2008.

[13] R. Morales-caporal, S. Member, M. Pacas, and S. Member, "A Predictive Torque Control Of Synchronous Reluctance Machine Taking Into Account the Magnetic Cross Saturation," IEEE Trans. Ind. Electron., vol. 54, no. 2, pp. 1161–1167, 2007.

[14] M. Pacas and J. Weber, "Predictive Direct Torque Control for the PM Synchronous Machine," IEEE Trans. Ind. Electron., vol. 52, no. 5, pp. 1350–1356, 2005.

[15] S. A. Davari, D. A. Khaburi, and R. Kennel, "An improved FCS-MPC algorithm for an induction motor with an imposed optimized weighting factor," IEEE Trans. Power Electron., vol. 27, no. 3, pp. 1540–1551, 2012.

[16] S. A. Davari, D. A. Khaburi, F. Wang, and R. M. Kennel, "Using full order and reduced order observers for robust sensorless predictive torque control of induction motors," IEEE Trans. Power Electron., vol. 27, no. 7, pp. 3424–3433, 2012.

[17] X. Xiao and C. M. Chen, "Reduction of Torque Ripple Due to Demagnetization in PMSM Using Current Compensation," IEEE Trans. Appl. Supercond., vol. 20, no. 3, pp. 1068–1071, 2010.

[18] K. Y. Cho, J. D. Bae, S. K. Chung, and Y. M. J., "Torque harmonics minimisation in permanent magnet synchronous motor with back EMF estimation," IEE Proc.-Electr Power Appl., vol. 141, no. 6, pp. 323–330, 1994.

[19] P. Kshirsagar and R. Krishnan, "High-efficiency current excitation strategy for variable-speed

nonsinusoidal back-EMF PMSM machines," IEEE Trans. Ind. Appl., vol. 48, no. 6, pp. 1875–1889, 2012.
[20] D. Luenberger, "An introduction to observers," IEEE Trans. Automat. Contr., vol. 16, no. 6, pp. 596–602, 1971.
[21] C. Schauder, "Adaptive speed identification for vector control of induction motors without rotational transducers," IEEE Trans. Ind. Appl., vol. 28, no. 5, pp. 1054–1061, Sep./Oct. 1992.
[22] M. Tursini, "Adaptive sliding-mode observer for speed-sensorless control of induction motors," IEEE Trans. Ind. Appl., vol. 36, no. 5, pp. 1380–1387, 2000.
[23] Y.-R. Kim, S.-K. Sul, M.-H. Park, I. Motor, and U. Extended, "Speed sensorless vector control of induction motor using extended Kalman filter," Ind. Appl. IEEE Trans., vol. 30, no. 5, pp. 1225–1233, 1994.
[24] L. Qian, D. A. Cartes, and H. Li, "An Improved Adaptive Detection Method for Power Quality Improvement," Industry Applications, IEEE Transactions on, vol. 44, no. 2. pp. 525–533, 2008.
[25] F. D. Freijedo, J. Doval-Gandoy, O. Lopez, P. Fernandez-Comesana, and C. Martinez-Penalver, "A Signal-Processing Adaptive Algorithm for Selective Current Harmonic Cancellation in Active Power Filters," Industrial Electronics, IEEE Transactions on, vol. 56, no. 8. pp. 2829–2840, 2009.
[26] B. Singh and J. Solanki, "An Implementation of an Adaptive Control Algorithm for a Three-Phase Shunt Active Filter," Industrial Electronics, IEEE Transactions on, vol. 56, no. 8. pp. 2811–2820, 2009.
[27] M. Cirrincione, M. Pucci, G. Vitale, and A. Miraoui, "Current Harmonic Compensation by a Single-Phase Shunt Active Power Filter Controlled by Adaptive Neural Filtering," Industrial Electronics, IEEE Transactions on, vol. 56, no. 8. pp. 3128–3143, 2009.
[28] R. R. Pereira, C. Henrique, L. Eduardo, G. Lambert-torres, and J. O. P. Pinto, "New Strategies for Application of Adaptive Filters in Active Power Filters," IEEE Trans. Ind. Appl., vol. 47, no. 3, pp. 1136–1141, 2011.
[29] L. Tong, X. Zou, S. Feng, Y. Chen, Y. Kang, Q. Huang, and Y. Huang, "An SRF-PLL-based sensorless vector control using the predictive deadbeat algorithm for the direct-driven permanent magnet synchronous generator," IEEE Trans. Power Electron., vol. 29, no. 6, pp. 2837–2849, 2014.
[30] G. Wang, T. Li, G. Zhang, X. Gui, D. Xu, and S. Member, "Position Estimation Error Reduction Using Recursive-Least-Square Adaptive Filter for Model-Based Sensorless Interior Permanent-Magnet Synchronous Motor Drives," IEEE Trans. Ind. Electron., vol. 61, no. 9, pp. 5115–5125, 2014.
[31] P. Niazi and H. a Toliyat, "Robust Maximum Torque per Amp (MTPA) Control of PM-Assisted Synchronous Reluctance Motor," IEEE Appl. Power Electron. Conf. Expo. APEC, pp. 685–692, 2006.
[32] A. K. Chakali, H. a. Toliyat, and H. Abu-Rub, "Observer-based sensorless speed control of PM-assisted SynRM for direct drive applications," IEEE Int. Symp. Ind. Electron., no. 3, pp. 3095–3100, 2010.
[33] I. Boldea, C. I. Pitic, C. Lascu, G. D. Andreescu, L. Tutelea, F. Blaabjerg, and P. Sandholdt, "DTFC-SVM motion-sensorless control of a PM-assisted reluctance synchronous machine as starter-alternator for hybrid electric vehicles," IEEE Trans. Power Electron., vol. 21, no. 3, pp. 711–719, 2006.
[34] S. Bolognani, L. Tubiana, and M. Zigliotto, "Extended Kalman filter tuning in sensorless PMSM drives," IEEE Trans. Ind. Appl., vol. 39, no. 6, pp. 1741–1747, 2003.
[35] S. Bolognani, M. Zigliotto, and M. Zordan, "Extended-range PMSM sensorless speed drive based on stochastic\nfiltering," IEEE Trans. Power Electron., vol. 16, no. 1, pp. 110–117, 2001.
[36] P. Guglielmi, M. Pastorelli, G. Pellegrino, and A. Vagati, "Position-Sensorless Control of Synchronous Reluctance Motor," Ind. Appl. IEEE Trans., vol. 40, no. 2, pp. 615–622, 2004.
[37] F. Genduso, R. Miceli, C. Rando, and G. R. Galluzzo, "Back EMF sensorless-control algorithm for high-dynamic performance PMSM," IEEE Trans. Ind. Electron., vol. 57, no. 6, pp. 2092–2100, 2010.
[38] K. Q. Nguyen, T. H. Nguyen, and Q. P. Ha, "FPGA-Based Sensorless PMSM Speed Control using Reduced-Order Extended Kalman Filters," IEEE Trans. Ind. Electron., vol. 0046, no. c, pp. 1–1, 2014.
[39] S. Ichikawa, M. Tomita, S. Doki, and S. Okuma, "Sensorless control of permanent-magnet synchronous motors using online parameter identification based on system identification theory," IEEE Trans. Ind. Electron., vol. 53, no. 2, pp. 363–372, 2006.